Journal of The Electrochemical Society, **152** (2) A333-A342 (2005)
0013-4651/2004/152(2)/A333/10/$7.00 © The Electrochemical Society, Inc.

Adaptive Energy Management of Electric and Hybrid Electric Vehicles

Mark Verbrugge,*,z Damon Frisch, and Brian Koch

General Motors Corporation, Warren, Michigan 48090, USA

An adaptive algorithm based on weighted recursive least squares is derived and implemented. The generality of the approach is underscored by the application of the algorithm to a 42 V lead acid and a high-voltage (375 V) nickel metal hydride battery system. The algorithm is fully recursive in that the only variables required for on-line regression are those of the previous time step and the current time step. A time-weighting technique often referred to as exponential forgetting is employed to damp exponentially the influence of older data on the regression analysis. The output from the adaptive algorithm is the battery state of charge (remaining energy), state of health (relative to the battery's nominal rating), and power capability. Such algorithms are likely to play a critical role in optimal operation of hybrid electric vehicles and on-board diagnostics. The behavior of the algorithm in terms of convergence, accuracy, and robustness is examined.
 [DOI: 10.1149/1.1847658]

Manuscript submitted May 28, 2004; revised manuscript received July 2, 2004. Available electronically December 23, 2004.

In a previous work,[1] the challenges and motivation behind determining a battery's state of charge (SOC), state of health (SOH), and power capability for both discharge and charge were described. The SOC corresponds to the stored charge available to do work relative to that available after the battery has been fully charged, and it can be viewed as a thermodynamic quantity. SOH refers to how well the battery system is functioning relative to its nominal (rated) and end (failed) states. Results presented in this work indicate that adaptive acquisition of the high-frequency resistance of the battery system can be used to assess the SOH.

For hybrid electric vehicles, algorithms represent the core piece of the value chain for software and control processes. Reviews on the substantially interdependent fields of recursive identification, adaptive filters, optimal estimators, and model-reference adaptive systems can be found in Ref. 2-7. Regarding automotive propulsion systems, most texts covering control theory treat motor control and feedback systems associated with vehicle speed control; little attention has been given to the adaptive control of battery systems.[8] This work bridges two very different fields: electrochemistry and adaptive controls. The electrochemical theory is needed to construct a model of the plant (the battery system), here in the form of an electrical equivalent circuit. Control theory is employed to regress, adaptively and efficiently, parameters associated with the electrochemical model so that the state of the battery system can be estimated. More specifically, this paper provides a detailed examination of a weighted recursive least-squares (WRLS) algorithm; unlike the algorithm described in Ref. 1, wherein a least-squares analysis was completed on a fixed frame of data points (corresponding to ''Window function''), the algorithm described in this work is more sophisticated in that all data points recorded are included in the on-line regression, and exponential forgetting[2-7] is incorporated to emphasize continuously the larger influence of the most recent data points on the SOC, SOH, and power capability regressions.[9] The wide-ranging applicability of the approach is underscored by the application of the algorithm to a 42 V lead acid battery and a high-voltage (375 V) nickel metal hydride (NiMH) system.

Experimental

Lead acid experiments.—Laboratory experiments were conducted with individual 12 V Panasonic HV1255 valve-regulated lead-acid (VRLA) batteries [GM part no. EC-HV1255 V (12 V)] of 55 Ah rated capacity. Cycling was performed with an AeroVironment MT30 cycler. The voltage was measured with 0.125 V accuracy and 0.03 V resolution, and the current was measured with an accuracy of −0.175 A or 0.25% of the reading (whichever was greater) and a resolution of 0.03 A. Voltage measurements were made at the battery terminals using a separate high-impedance input to the cycler to eliminate line voltage drop. Battery power *vs.* time traces from actual hybrid vehicle operation were supplied to the cycler as command inputs for cycling the batteries. Peak power tests were conducted by commanding constant voltage.

NiMH experiments.—Laboratory testing was conducted with a high-voltage, liquid-cooled battery pack. The pack was composed of 26 NiMH modules (SAFT version 12.1), each with a nominal voltage of 12 V and a rated capacity of 96 Ah. Voltage, current, and temperature data were collected at 1 s intervals from the battery pack controller. Module voltage was measured with 0.1 V accuracy and 0.01 V resolution. Pack current was measured by a shunt with an accuracy of 0.25 A over the range of −40 to +40 A, and an accuracy of 13 A for all other values. The pack current resolution was 0.1 A. The battery terminal temperature was measured by thermistors at several locations in the pack with an accuracy of 1°C and a resolution of 0.2°C. Cycling was performed with an AeroVironment ABC-150 cycler. The cycler voltage was measured with an accuracy of 0.25 V, and the current was measured with an accuracy of 0.2 A or 0.25% of the reading, whichever was greater. Power *vs.* time profiles at intervals of 1 s were provided to the cycler as command inputs.

Vehicle testing was performed with an S-10E electric vehicle powered by the same SAFT NiMH battery pack used for the laboratory tests. The battery was discharged (via an inverter) through the vehicle's 75 kW ac induction motor to provide propulsion. The same system provided regenerative braking energy to charge the battery. Data was collected at 1 s intervals from the battery pack controller over the vehicle serial data bus.

Model Formulation

The basic structure of an adaptive transversal filter is shown in Fig. 1. Rather than store, recall, and reweight each collected data point to construct the filter in an on-line application, recursive formulations employing only quantities from previous and present time steps are highly preferred for embedded controllers.[2-7] In this section, we develop an electrochemical model that can be transformed into a WRLS formulation; the final WRLS model is functionally equivalent to an adaptive transversal filter but is fully recursive. In addition, all ancillary calculations (*e.g.*, a skewness test of the excitation source to determine if the data stream is appropriate for regression analysis) are formulated to be fully recursive.

The model used for this estimation system consists of two parts. An electrical circuit model is employed to describe the relationship between the currents and voltages observed at the terminals of the battery (giving rise to the voltage-based SOC_V, cf. Fig. 2 and 3 for the VRLA batteries corresponding to the experimental results of this work), and a coulomb-accumulation model is used to describe the

* Electrochemical Society Active Member.
z E-mail: mark.w.verbrugge@gm.com

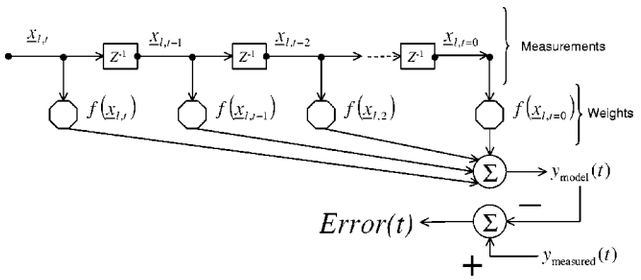

Figure 1. Adaptive transversal filter.[4] The unit delay function is represented by z^{-1}. The measured temperature and current is represented by x_1. A model is used to construct the weights (here an equivalent circuit model of a battery system). The measured voltage corresponds to y_{measured}; y_{model} is the modeled voltage. A recursive relation removes the need to sequentially go back in time beyond the previous time step in order to obtain data to extract parameter values.

open-circuit voltage (OCV) based on the history of currents seen by the battery (giving rise to the coulomb-counting based SOC_C), which can include self-discharge and current inefficiency on charge. The electrical circuit model is illustrated in Fig. 4. Note that even the more complex equivalent circuit shown in the upper schematic of Fig. 4 constitutes a greatly simplified approach to modeling a battery system,[14-23] but the model is useful for the purposes of an adaptive transversal filter. Because the SOC is a function of the open-circuit potential (OCP), extraction of the OCV by least-squares regression leads to an estimate of the SOC. Both SOC_V and SOC_C yield useful information regarding the SOC; thus a composite SOC value is calculated[1,12]

$$SOC = w_{\text{SOC}}(SOC_C) + (1 - w_{\text{SOC}})(SOC_V) \qquad [1]$$

where w_{SOC} is a weighting factor, SOC_C is the SOC as calculated by coulomb integration, and SOC_V corresponds to a voltage-based SOC to be described later. For SOC_C

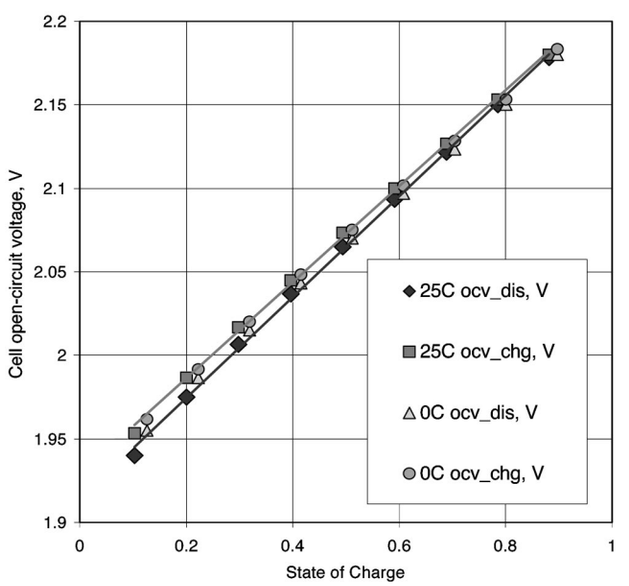

Figure 2. OCP.[10] These data correspond to the measured OCV collected 15 min after a sustained discharge (dis) or charge (chg). For temperatures up to about 45°C, the OCV curve does not differ significantly from the 25°C curves shown.

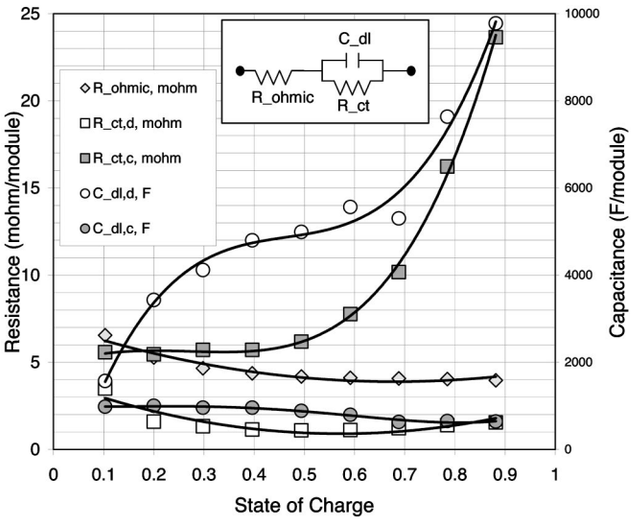

Figure 3. Parameter regression from experimental results.[10,11] These values can be used to start adaptive algorithms and set bounds on parameter values. The high-frequency resistance corresponds to R_ohmic in the plot.

$$SOC_C(t) = SOC(t - \Delta t) - \int_{t-\Delta t}^{t} \left[100 \frac{\eta_I I}{Ah_{\text{nominal}}} + S_D(T, SOC) \right] \frac{dt}{3600} \qquad [2]$$

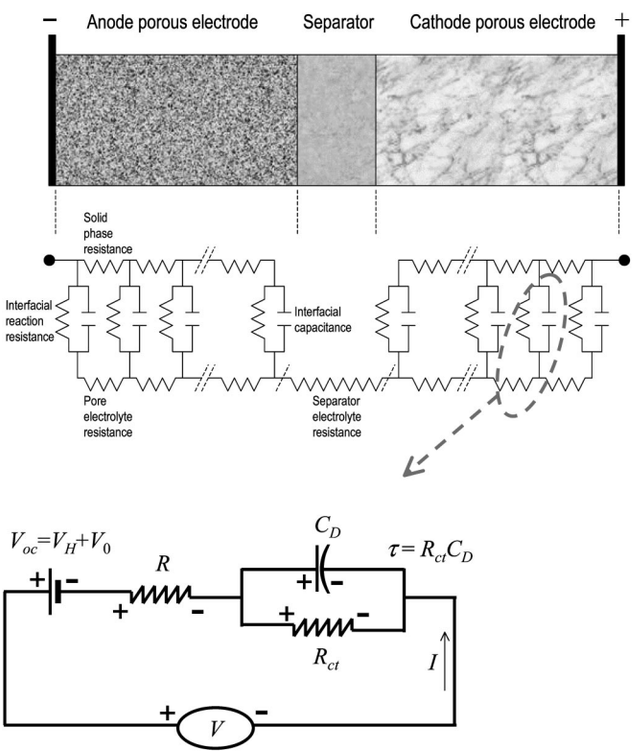

Figure 4. Equivalent circuit for a battery and that used in the adaptive algorithm.[10,12,13] The dotted arrow and oval indicate that a small portion of the larger equivalent circuit is used in the adaptive algorithm to represent the battery system. (Note that the more complex equivalent circuit shown in the upper schematic constitutes a greatly simplified approach to modeling a battery system.[22])

Time is represented by t and I denotes current; discharge currents are taken as positive. For the lead-acid module of this example, the nominal capacity Ah_{nominal} corresponds to the ampere-hours of capacity the battery delivered when discharged from 100% SOC to 0% SOC at the C/3 rate; *i.e.*, at a current that discharges the nominal capacity in 3 h. (When the algorithm is used to treat an electric vehicle (EV) NiMH system, the relevant parameters are specified; most of this publication is based on the 42 V lead-acid battery pack.) For SOC algorithms, the self-discharge rate can be tabulated as a function of temperature and SOC based on experimental measurements. The current efficiency η_I is effectively unity for the conditions at or below 70% SOC and declines to zero as full charge is obtained and secondary electrochemical reactions are initiated upon further charging. Generally, current efficiencies are expected to have a mild temperature dependence and decrease with increasing SOCs. (See Ref. 24 and 25 for the effect of gassing in lead-acid batteries and its influence on the current voltage response.) The factor 3600 has units of s/h, and the factor 100 is employed to keep a consistent percent basis. For all the analyses to be discussed in this work, neither the self-discharge rate nor the current efficiency substantially affects the results, and it is sufficient to view $S_D = 0$ and $\eta_I = 1$.

To extract the voltage-based SOC_V, the model corresponding to the equivalent circuit shown in the lower schematic of Fig. 4 is employed. For any arbitrary current source, the voltage is given by[12,13,26]

$$V = V_{oc} - IR + A\int_{\zeta=t}^{\zeta=0} I(\zeta)\exp[-B(t-\zeta)]d\zeta \qquad [3]$$

The first two terms on the right side give rise to an ohmic description of the battery, as the battery voltage V is related to the V_{oc} reduced by the ohmic drop IR, where R is the battery resistance. Relative to the equivalent circuit in Fig. 4, $A = 1/C_D$ and $B = 1/(C_D R_{ct})$. The last term on the right side corresponds to a superposition integral, through which past currents influence the OCP beyond the first-order effect of changing the average state of charge characterizing the electrodes. (Because of the exponential weighting function, the impact of older current-potential data points is exponentially less than that of recent data points. Note that for the application of Eq. 3, ζ is the dummy variable of integration.)

The V_{oc} is a function of temperature, SOC, and a hysteresis function

$$V_{oc,cell} = \text{function}(T, SOC, V_H) = V_{0,cell}(T, SOC) + V_H \qquad [4]$$

The quantity $V_{0,cell}$ is nearly linear for lead-acid batteries (cf. Fig. 2). For the hysteresis contribution, we construct the following first-order differential equation to calculate a hysteresis voltage V_H[1]

$$\frac{\partial V_H}{\partial t} = -\beta(\eta_I I - \varepsilon S_D)[V_{H,max} + \text{sign}(I)V_H] \qquad [5]$$

This equation constructs a varying hysteresis voltage. For the lead-acid battery of this study, the hysteresis voltage is set up so that for prolonged charge currents, or short but very large charge currents, the hysteresis voltage tends to $V_{H,max} = 16.5$ mV per cell by selecting the appropriate parameter values. The exact opposite holds for discharge (positive) currents. Note also that if the current remains at zero for a long time, the hysteresis voltage tends to the charge-decreasing condition (−16.5 mV per cell) through self-discharge (provided $\varepsilon \neq 0$). In general, voltage hysteresis plays a minor role in the lead-acid system; the 16.5 mV/cell hysteresis voltage, 2.1 V/cell nominal OCV, and a linear variation in OCV with SOC for the lead-acid system can be contrasted with 50 mV/cell hysteresis voltage, 1.3 V/cell nominal OCV, and little variation in OCV with SOC for the NiMH system.[13,26] For this work, all results correspond to $\varepsilon = 0$, $\eta_I = 1$, and $\beta = 1.12 \times 10^{-4}$ C^{-1} (for both charge and discharge).

Implementation

To implement the preceding system of equations, a discretized, recursive formulation is required. We begin with the coulomb integration model for SOC_C

$$SOC_C(t) = SOC(t - \Delta t) - \left[100\frac{[(\eta_I I_{t-1} + \eta_I I_t)/2]}{Ah_{\text{nominal}}} + (S_D)_{t-\Delta t}\right]\frac{\Delta t}{3600} \qquad [6]$$

Note that the integration over a time interval begins at SOC, not SOC_C. The difference between the present time and the last recorded time is given by Δt. Next, the measured voltage is corrected for the superposition integral. First, it is helpful to note that Eq. 3 can be recast as the following recursion relation for evaluation purposes

$$V|_t = (V_{oc} - IR)_t - \left(\frac{I|_t + I|_{t-\Delta t}}{2}\right)A\Delta t + \exp(-B\Delta t)[V - (V_{oc} - IR)]_{t-\Delta t} \qquad [7]$$

where the subscripts t and $t - \Delta t$ denote the time at which the quantities are to be evaluated. This equation and its derivation are similar to that presented in the Appendix of Ref. 1; however, for this expression, the current source is averaged over the time step, giving a more accurate approximation to Eq. 3. Note that consistent with all recursion relations, only variables calculated at the previous time step are required to calculate the voltage at time t. To implement Eq. 7 for our two-parameter algorithm, we replace the battery voltage with measured values and formulate a regression voltage

$$V^{\text{regression}} = V^{\text{measured}}|_t + \left(\frac{I|_t + I|_{t-\Delta t}}{2}\right)A\Delta t - \exp(-B\Delta t) \times [V^{\text{measured}} - (V_{oc} - IR)]_{t-\Delta t} = (V_{oc} - IR)_t \qquad [8]$$

Thus, the regression analysis to determine the OCP and resistance is based on the voltage quantity appearing on the left side, the regression voltage, and a least-squares analysis of the corrected voltage data (corresponding to the regression voltage) should yield a good approximation for the ohmic resistance and OCP. Next the V_{oc} and the resistance R are extracted from the corrected battery voltage regression voltage $V^{\text{regression}}$ and measured current I. This extraction procedure is based on a recursive least-squares approach, which is now derived.

WRLS formulation.—We intend to minimize the error ξ by using a least-squares regression of V_{oc} and R

$$\xi = \sum_{j=1}^{j=N} [y_j - (mx_j + b)]^2 \qquad [9]$$

where ξ is the error and the model ($y = mx + b$) of the physical system is linear.

Consistent with Eq. 8, the slope m corresponds to the high-frequency resistance R, and the intercept b corresponds to the V_{oc} (from which we extract the SOC after the hysteresis contribution has been removed); x_j corresponds to the measured currents, and y_j corresponds to the regression voltage $V^{\text{regression}}$. Two equations for the two unknowns m and b can be obtained by taking the first derivatives in ξ with respect to the two unknowns and setting the first derivatives to zero

$$\frac{\partial \xi}{\partial b} = \sum_{j=1}^{j=N} (-2)(y_j - mx_j - b) = 0 \text{ leads to}$$

$$b = -\frac{1}{N}\sum_{j=1}^{j=N} y_j - \frac{1}{N}m\sum_{j=1}^{j=N} x_j$$

and

$$\frac{\partial \xi}{\partial m} = \sum_{j=1}^{j=N} (-2x_j)(y_j - mx_j - b) = 0 \text{ leads to}$$

$$0 = \sum_{j=1}^{j=N} x_j y_j - m\sum_{j=1}^{j=N} x_j^2 - b\sum_{j=1}^{j=N} x_j$$

These equations can be used to derive the following expressions for m and b

$$m = \frac{\Sigma_{j=1}^{j=N} x_j y_j - \frac{1}{N}\Sigma_{j=1}^{j=N} x_j \Sigma_{j=1}^{j=N} y_j}{\Sigma_{j=1}^{j=N} x_j^2 - \frac{1}{N}(\Sigma_{j=1}^{j=N} x_j)^2}$$

$$\text{and } b = \frac{1}{N}\left(\sum_{j=1}^{j=N} y_j - m\sum_{j=1}^{j=N} x_j\right) \quad [10]$$

To make this system fully recursive, we recognize that each sum can be constructed from its previous value and its current value, *e.g.*

$$\sum_{j=1}^{N} x_j = x_j + \sum_{j=1}^{N-1} x_j$$

We now recast Eq. 9 to formulate a WRLS approach. For exponential forgetting and weighting of charge and discharge differently, we assume that the parameters m and b change slowly with time and introduce a weighting factor w_j

$$\xi = \sum_{j=1}^{N} w_j[y_j - (mx_j + b)]^2 \quad [11]$$

where preferential weighting of discharge over charge is accomplished by

$$w_j = \gamma_j \lambda^{N-j} \quad \begin{cases} \gamma_j = 1, & \text{charge} \\ \gamma_j > 1, & \text{discharge} \end{cases} \quad [12]$$

The exponential forgetting factor corresponds to λ,[2-7] and γ_j is the charge-discharge weight factor. It can be shown that the use of λ^{N-j} yields an exponential decay in the influence of past points on the determination of the current value of m and b

$$\lambda^{N-j} = e^{\ln \lambda^{N-j}} = e^{(N-j)\ln \lambda} \approx e^{(N-j)(\lambda - 1)} \quad \text{for } \lambda \to 1 \quad [13]$$

The following definitions are utilized

$$s_I = \frac{1}{\Sigma_{j=1}^{N} w_j}\sum_{j=1}^{N} w_j I_j$$

$$s_{II} = \frac{1}{\Sigma_{j=1}^{N} w_j}\sum_{j=1}^{N} w_j I_j^2$$

$$s_V = \frac{1}{\Sigma_{j=1}^{N} w_j}\sum_{j=1}^{N} w_j V_j^{\text{regression}}$$

$$s_{IV} = \frac{1}{\Sigma_{j=1}^{N} w_j}\sum_{j=1}^{N} w_j I_j V_j^{\text{regression}}$$

where N represents the number of recorded current-potential data points to be included in the extraction of the V_{oc} and the resistance. Using these expressions, we can write the following

$$R = -\frac{s_{IV} - s_I s_V}{s_{II} - (s_I)^2} \quad [14]$$

and

$$V_{oc} = \frac{s_{II} s_V - s_{IV} s_I}{s_{II} - (s_I)^2} \quad [15]$$

The remaining manipulations recast these equations into the fully recursive form as indicated previously. Specifically, by straightforward algebraic manipulation, the following equations are derived; in application, the first equation is to be implemented prior to the following four at each time step

$$s_w|_N = \sum_{j=1}^{N} w_j = \sum_{j=1}^{N} \gamma_j \lambda^{N-j} = \gamma_N + \lambda\sum_{j=1}^{N-1} \gamma_j \lambda^{N-1-j} = \gamma_N + \lambda(s_w|_{N-1})$$

$$s_I|_N = \frac{1}{\Sigma_{j=1}^{N} w_j}\sum_{j=1}^{N} w_j I_j = \frac{\gamma_N I_N + \lambda(s_I|_{N-1})(s_w|_{N-1})}{(s_w|_N)}$$

$$s_{II}|_N = \frac{1}{\Sigma_{j=1}^{N} w_j}\sum_{j=1}^{N} w_j I_j^2 = \frac{\gamma_N I_N^2 + \lambda(s_{II}|_{N-1})(s_w|_{N-1})}{(s_w|_N)}$$

$$s_V|_N = \frac{1}{\Sigma_{j=1}^{N} w_j}\sum_{j=1}^{N} w_j V_j^{\text{regression}} = \frac{\gamma_N V_N^{\text{regression}} + \lambda(s_V|_{N-1})(s_w|_{N-1})}{(s_w|_N)}$$

$$s_{IV}|_N = \frac{1}{\Sigma_{j=1}^{N} w_j}\sum_{j=1}^{N} w_j I_j V_j^{\text{regression}} = \frac{\gamma_N I_N V_N^{\text{regression}} + \lambda(s_{IV}|_{N-1})(s_w|_{N-1})}{(s_w|_N)}$$

Thus, the far right term in each of these five equations allows one to determine the indicated sum by considering values at the time step N and calculated values from the previous time step: these are fully recursive expressions. Another useful feature of these equations is that although exponential forgetting is embedded within the system, no exponentiation that could lead to underflow or overflow errors results in the equation system. Care must be exercised in starting up recursive routines; the following expressions are used for $N = 1$ (the first time step)

$$s_w|_1 = \gamma_1$$

$$s_I|_1 = \gamma_1 I_1$$

$$s_{II}|_1 = \gamma_1 I_1^2$$

$$s_V|_1 = \gamma_1 V_1$$

$$s_{IV}|_1 = \gamma_1 I_1 V_1$$

A variance test is important to determine the quality of the data for regression analysis and to avoid the division by zero associated with singular equation systems and an excessively small determinant for a matrix system of equations. The denominator term can be shown to be a variance;[27] thus we define

$$\textit{denom\_test} = \begin{cases} 1 & \text{if } s_{II} - (s_I)^2 \geqslant \underline{0.5\ \text{A}} \\ 0 & \text{if } s_{II} - (s_I)^2 < \underline{0.5\ \text{A}} \end{cases} \quad [16]$$

Underlined values represent suggested calibrations for the 42 V lead-acid battery pack; these calibrated values were used in this work. A value of unity reflects passage of the denominator (determinant) test.

We next describe a recursive skewness test. For our purposes, we define skewness as[27]

$$skewness = \left| \frac{1}{N\sigma^3} \sum_{j=1}^{j=N} (x_j - \overline{x})^3 \right| \quad [17]$$

where $\overline{x}$ is the average of the x-values ($\overline{x} = s_I$) and σ^2 is a variance ($\sigma^2 = s_{II} - s_I^2$). We restrict the skewness test to the actual current-time values and do not incorporate the charge-discharge weighting. Following the same logic used previously, the following summations and recursive relations are derived; the subscript s is added to indicate quantities associated with the skewness calculation

$$s_{w,s}|_N = \sum_{j=1}^{N} \lambda^{N-j} = 1 + \lambda \sum_{j=1}^{N-1} {}_j\lambda^{N-1-j} = 1 + \lambda(s_{w,s}|_{N-1})$$

$$s_{I,s}|_N = \frac{1}{\sum_{j=1}^{N}\lambda^{N-j}} \sum_{j=1}^{N} \lambda^{N-j} I_j = \frac{I_N + \lambda(s_{I,s}|_{N-1})(s_{w,s}|_{N-1})}{(s_{w,s}|_N)}$$

$$s_{II,s}|_N = \frac{1}{\sum_{j=1}^{N}\lambda^{N-j}} \sum_{j=1}^{N} \lambda^{N-j} I_j^2 = \frac{I_N^2 + \lambda(s_{I,sI}|_{N-1})(s_{w,s}|_{N-1})}{(s_{w,s}|_N)}$$

$$skewness|_N = \begin{cases} skew\_cal & \text{if } denom\_test \leqslant 0 \\ \left[\dfrac{\left| \dfrac{(I_N - s_{I,s}|_N)^3}{[s_{II,s}|_N - (s_{I,s}|_N)^2]^{3/2}} \right| + (skewness|_{N-1})(N-1)}{N} \right] & \text{if } denom\_test > 0 \end{cases}$$

The value of *skew_cal* represents a calibration. A large value may be more appropriate if it is desired to start the WRLS portion of the algorithm sooner ($skew\_cal = 10$ was used in this work). To start the recursive calculations for skewness, the following conditions are used

$$s_{w,s}|_1 = 1$$

$$s_{I,s}|_1 = I_1$$

$$s_{II,s}|_1 = I_1^2$$

Analogous to *denom_test*, define

$$skew\_test = \begin{cases} 0 & \text{if } skewness \geqslant skew\_cal \\ 1 & \text{if } skewness < skew\_cal \end{cases}$$

As with *denom_test*, the regression analysis is not employed if the skew test is not passed. When either *skew_test* or *denom_test* or both are zero, and the regression analysis is not implemented, the OCV is found by

$$V_{oc} = V^{measured}|_t + (I|_t R|_{t-\Delta t}) + \left(\frac{I|_t + I|_{t-\Delta t}}{2} \right) A\Delta t - \exp(-B\Delta t)[V^{measured} - (V_{oc} - IR)]_{t-\Delta t} \quad [18]$$

where it is seen that the employed resistance R is taken from the previous time step value.

Evaluation of the voltage-based SOC.—The preceding discussion shows how to extract an estimate for the OCV; it now remains to convert this estimate into SOC_V, and for this the hysteresis voltage must be treated. For the time integration, the following is applied[1]

$$V_H(t) = w_H\{V_H - (\Delta t)\beta[\eta_I I + S_D]\}_{t-\Delta t} + (1 - w_H)[V_{oc,cell} - V_0(T, SOC_V)]_{t-\Delta t} \quad [19]$$

Although the subscript on the brackets and braces indicates that values to the right of this equation can be evaluated at the previous time step, note that the current is known (measured) for all times, so the current employed (and the current efficiency) can be taken as the average of the present and previous time steps to increase accuracy. It is also important to note that this equation is not a straightforward time integration of Eq. 5 unless the weighting factor w_H is set to unity. Thus, the quantity $[V_{oc,cell} - V_0(T, SOC_V)]_{t-\Delta t}$ in Eq. 19 allows for a correction to the extraction of the hysteresis voltage through the recognition that the previous time step value for the SOC can be used to calculate an OCV. This back-calculated OCV provides a value of V_H that likely differs from that calculated using Eq. 5 alone.

The next step is to transform the V_{oc} into a voltage-based SOC, including the hysteresis voltage. Because we can now calculate $V_0(T, SOC_V) = V_{oc} - V_H$, we can simply invert $V_0(T, SOC_V)$ to extract SOC_V. For lead-acid, the approximately linear relation depicted in Fig. 2 can be employed. For example, at 25°C

$$V_{oc}(\text{volts/cell, } 25°C) = 1.9214 + 0.2949\frac{SOC}{100}$$

for the lead-acid batteries of this work. Finally, as noted initially, the combined SOC can now be calculated from Eq. 1; *i.e.*, $SOC = w_{SOC}(SOC_C) + (1 - w_{SOC})(SOC_V)$. The next section addresses the weight factors w_{SOC} and w_H.

Specification of w_{SOC} and w_H.—An important topic to be clarified is the weight factors w_{SOC} and w_H; the influence of the time step size must be addressed in the calculation of these factors as well. That is, if very small time steps are employed, then the weighting factor should be altered so that time-dependent quantities are not lost from the calculation and instead are allowed to evolve in accordance with their particular time constants. Thus the following approach is applied in this example application[1,12]

$$w_{SOC} = w_{SOC,max} - \alpha_w(\Delta t) \quad \text{and} \quad w_H = w_{H,max} - \alpha_H(\Delta t) \quad [20]$$

These weighting factors are to be bounded (*e.g.*, between 0.5 and 1). We provide an overview of what must be considered in specifying w_{SOC} and w_H, but application of the algorithm in an operating environment (algorithm tuning[2]) must be exercised to find the appropriate values for a specific application. For w_H, because the lead-acid battery does not exhibit significant hysteresis effects, we set $w_H = 1$ throughout; that is, the hysteresis voltage is calculated and included in the results, but it is not adapted (cf. Eq. 19).

When the battery SOC exceeds about 95%, the voltage-based SOC can become inaccurate due to the less predictable processes associated with the overcharge reactions discussed previously. Similarly, for short times (*i.e.*, before the regression analysis allows for accurate fitting of the resistance and OCP), w_{SOC} can be set to unity, and the SOC is calculated for this short time based solely on coulomb integration provided the initial SOC is known (*e.g.*, stored in the embedded controller memory and corrected for self-discharge or initialized prior to power excitation from the measured value of V_{oc}). Another special case results when the battery has been at rest for prolonged periods. In this case, the hysteresis model returns a value of V_H that is less than −10 mV, and the magnitude of the current is quite low (*e.g.*, less than 0.01 A). In this case, the voltage-based SOC is likely to provide the most accurate estimate for the

combined SOC. We also desire that the voltage-based contribution be further enforced when the SOC falls below a calibrated value (20% is suggested) to avoid undervoltage faults that can impair the operation of devices requiring voltage values above a critical level.

Adaptive power capability.—The maximum discharge power can be expressed as

$$P_{\text{max,discharge}} = IV = IV_{\text{min}}$$

That is, when the battery voltage obtains its lowest acceptable value, the maximum discharge power results. First, consider an ohmic battery, wherein $V = V_{\text{oc}} - IR$, and

$$P_{\text{max,discharge}} = IV_{\text{min}} = \frac{(V_{\text{oc}} - V_{\text{min}})}{R} V_{\text{min}}$$

This expression corresponds to the high-frequency power capability and can be obtained by solving for the power capability associated with Fig. 4 when the capacitor is shorted out (offers no impedance) due to high-frequency excitation. Similarly, the high-frequency charge power for the ohmic battery corresponds to

$$P_{\text{max,charge}} = IV_{\text{max}} = \frac{(V_{\text{oc}} - V_{\text{max}})}{R} V_{\text{max}}$$

We shall refer to these power capabilities governed solely by the resistance R as instantaneous power capabilities. For the maximum ohmic resistance, obtained at long times, R is replaced by $R + R_{\text{ct}}$, where R_{ct} is often different for charge and discharge (cf. Fig. 3). In this low-frequency case, the power capability is associated with Fig. 4 and an open-circuited capacitor (infinite impedance) due to low-frequency excitation. Thus, the ohmic battery does not address transient effects such as those correlated by the superposition integral 3. To calculate the maximum charge and discharge powers available for the time interval Δt including capacitive effects, the current is obtained from Eq. 7

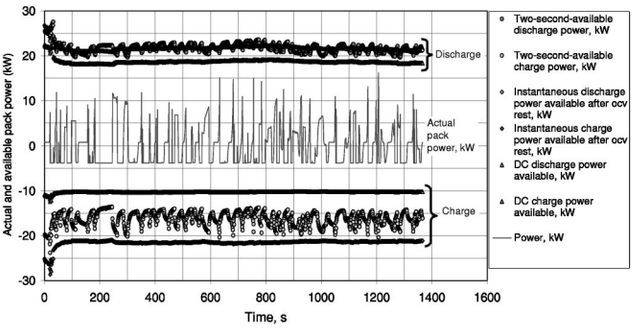

Figure 5. Pack power (measured independent variable) for the three-module pack (36/42 V system) and predicted available power capabilities.

Results and Discussion

The algorithm developed in the previous section was applied to two types of batteries: nominally 55 Ah lead-acid batteries used to construct GM's 42 V parallel hybrid truck (PHT) power source and 105 Ah NiMH batteries (SAFT) in an S10E EV modified for research and development purposes. Most of our effort is focused on the hybrid electric vehicle (HEV) application; the NiMH results are presented so as to determine whether the general approach can be used for both HEV and EV applications and on lead-acid and NiMH technologies.

Perhaps more than any other algorithm output, power capability is most important for HEV applications. The power capability plots shown in Fig. 5 for the 42 V battery pack result from the application of the algorithm using the power profile labeled ''Actual pack power, kW'' in Fig. 5 (along with a forgetting factor λ of 0.99 and unity for the discharge-to-charge weight factor γ_j for all points j, as shown in the base case curve of Fig. 6). The power on charge was kept under 4 kW, while discharge power pulses reached 15 kW. Analyzing Fig. 5, we see that after sustained charges (respectively discharges), the algorithm reports that the maximum charge (respectively discharge) power capability declines, while the maximum discharge (respectively charge) power capability increases. These observations are consistent with analyses of actual batteries and are directly attributable to transient irreversible losses that are simulated by the resistor-capacitor combination shown in Fig. 4. The effects are particularly evident between 200 and 300 s.

The weighting of the points ($w_j = \gamma_j \lambda$ per Eq. 12) is clarified in Fig. 6. We see that for the base case ($\gamma_j = 1$ for all points j and $\lambda = 0.99$), points older than about 100 s relative to the current data point (1341 s in Fig. 6) have a small (and exponentially decreasing) impact on the recursive least-squares regression. The far right curve in Fig. 6 shows that the relevant time window is reduced to about 10 s when λ is increased to 0.9, in agreement with Eq. 13. Last, changing the discharge-to-charge weight factor to $\gamma = 2$ results in discontinuous upper and lower weighting curves; values forming the upper curve correspond to discharge events (which receive twice the

$$I\big|_{\text{t}} = \frac{(V_{\text{oc}} - V)_{\text{t}} - (AI_{\text{t}-\Delta\text{t}}\Delta t/2) + \exp(-B\Delta t)[V - (V_{\text{oc}} + IR)]_{\text{t}-\Delta\text{t}}}{R + (A\Delta t/2)}$$

$$P_{\text{max,discharge}}\big|_{\text{t}} = IV_{\text{min}} = \left[\frac{(V_{\text{oc}} - V_{\text{min}})_{\text{t}} - (AI_{\text{t}-\Delta\text{t}}\Delta t/2) + \exp(-B\Delta t)[V - (V_{\text{oc}} + IR)]_{\text{t}-\Delta\text{t}}}{R + (AI_{\text{t}-\Delta\text{t}}\Delta t/2)}\right] V_{\text{min}} \quad [21]$$

$$P_{\text{max,charge}}\big|_{\text{t}} = IV_{\text{max}} = \left[\frac{(V_{\text{oc}} - V_{\text{max}})_{\text{t}} - (AI_{\text{t}-\Delta\text{t}}\Delta t/2) + \exp(-B\Delta t)[V - (V_{\text{oc}} + IR)]_{\text{t}-\Delta\text{t}}}{R + (AI_{\text{t}-\Delta\text{t}}\Delta t/2)}\right] V_{\text{max}}$$

To implement these equations, the respective powers are calculated immediately after the algorithm has been employed to finish the *SOC* determination at time t. In this case, quantities calculated or measured at time t are then immediately stored in the variables listed in the respective power expressions at time $t - \Delta t$. Then one must state the duration Δt corresponding to the desired estimate for power. (It would seem sufficiently accurate to not update V_{oc} unless Δt were to exceed tens of seconds. One could then use coulomb counting on the projected current to estimate a new state of charge and update V_{oc}.) For example, if we want to know the power estimates 2 s from the present time t, then the present measured and extracted values are placed in the $t - \Delta t$ subscripted quantities, t and Δt are set to 2 s, and the right sides of the preceding equations yield the desired maximum charge and discharge power estimates 2 s from the present.

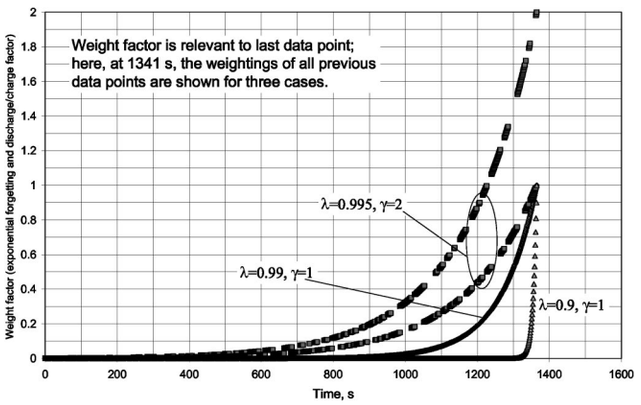

Figure 6. Weight factor components for weighted recursive least-squares formulation. Low values of λ are shown to weight preferentially the influence of more recent data. Two curves are seen when $\gamma \neq 1$; one for discharge data points and one for charge data points. When $\gamma > 1$ (respectively $\gamma < 1$), the curve for the discharge weight factor is above (respectively below) the charge curve. Note that for our base case ($\lambda = 0.99, \gamma = 1$), about 200 s of the most recent data are used to regress parameter values.

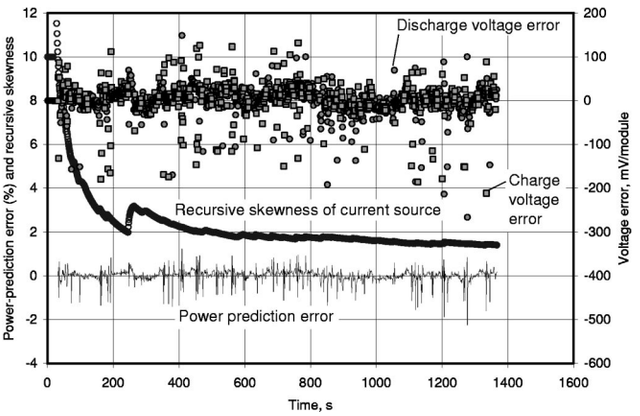

Figure 8. Statistics for weighted recursive least-squares regression associated with the power profile shown in Fig. 5. The power prediction error results from using the regressed values at time step $t - \Delta t$ to predict the power at time t given the current at time t *vs.* the actual power (current multiplied onto voltage) at time t.

weighting with $\gamma = 2$ and $w_j = 2\lambda$), while those forming the lower curve correspond to $w_j = \lambda_j$ on charge.

The remaining primary outputs from the algorithm are displayed in Fig. 7. The algorithm regresses the V_{oc} and high-frequency resistance R. For the lead-acid battery, the hysteresis voltage is included but is not adapted, as it does not play a large role. From the value of $V_0 = V_{oc} - V_H$, the voltage-based SOC_V is obtained (Eq. 4), which, when combined with coulomb counting, yields the extracted SOC (Eq. 1). For the rather short test durations of this work, pure coulomb counting can be used to access the SOC, unlike in actual continuous HEV operation, and the accuracy of the regressed SOC is reflected by the agreement between regressed SOC and the curve labeled $SOC_{\text{coulomb counting}}$. In addition, C/3 discharge of the battery at the end of the experiment yielded a capacity of 62% SOC, in close agreement with the regressed SOC. Generally, similar results were obtained when the SOC was cycled as in Fig. 7 about an average SOC value ranging from 40 to 70%.

The high-frequency resistance may be useful in assessing the health of the battery. This assertion is based on two observations.

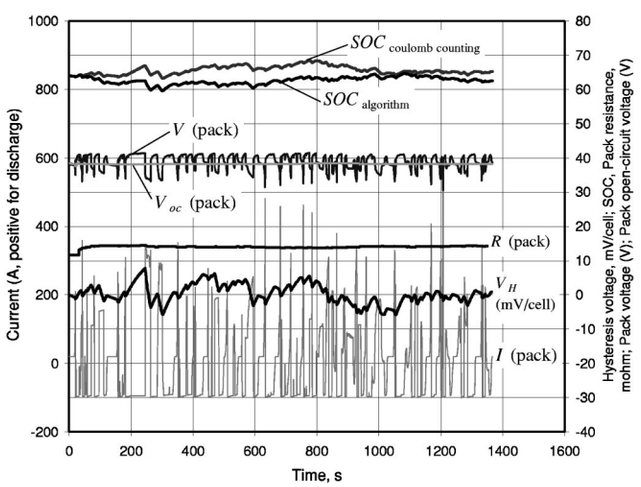

Figure 7. Measured pack voltage and current and SOC (by purely coulomb counting). Also shown are the calculated hysteresis voltage and the regressed SOC, OCV, and high-frequency pack resistance.

First, as electrodes degrade upon cycling, the intimate contact between conductive particles necessary for battery operation is slowly lost, resulting in larger values of R. Similarly, loss of acid due to sulfation (growth of inert lead sulfate crystals, removing sulfate ions from the electrolyte) leads to an increased ohmic resistance due to the loss of acid and a concomitant drop in electrolyte conductivity along with pore blockage attributable to the covering of otherwise active electrode reaction sites by inert lead sulfate crystals.[17] Similar phenomena take place in NiMH[28,29] and lithium-ion batteries; *i.e.*, upon cycling, the high-frequency resistance increases. We can anticipate that increases in high-frequency resistance upon extensive cycling can be expected for all commercially viable EV and HEV batteries.

Statistical aspects of the algorithm behavior based on the power profile displayed in Fig. 5 are plotted in Fig. 8 and 9. The error in representing the measured voltage using the regressed parameters is shown by the uppermost data in Fig. 8 and corresponds to $y_j - (mx_j + b)$ in Eq. 11. The time per point is 1 s for these data, and the power prediction error refers to the power predicted at time t when the parameters regressed from the previous timestep $t - \Delta t$ are used to calculate the battery voltage using the measured current at time t and Eq. 21. The error on charge and discharge was generally less than 100 mV/module, yielding usually less than 1% for both the voltage and power capability errors under these conditions. The immediate increase in the skewness of the current source near 245 s results from a nearly constant charge power excitation followed by an immediate change to discharge. The lower plot of Fig. 9 represents this skewed-data condition, whereas the upper plot corresponds to more random power excitation around 1021 s. The clustering of charge data in the lower plot (skewed data) of Fig. 9, relative to the upper plot, helps to explain why the regression statistics for the upper plot are superior to those of the lower plot.

Perhaps the most important aspect of Fig. 8 and 9 is that the plots help to explain why the algorithm works. When the parallel resistor-capacitor contribution to the impedance is removed from the measured voltage to form the regression voltage (cf. Eq. 8), the lowermost plot of Fig. 9 shows that a substantially linear relation holds for the resulting regression voltage *vs.* current, and one should expect the two-parameter linear regression to represent the data with little error. Note that the 91 points used to generate the plots shown in Fig. 9 correspond to 91 s, which is on the order of the duration of influence when $\lambda = 0.99$, the base-case value for the forgetting factor λ (cf. Fig. 6). Even when the data are skewed (lower plot of Fig. 9), the regression voltage *vs.* current is still linear; in implementation, we found that accepting all data for regression when the skew-

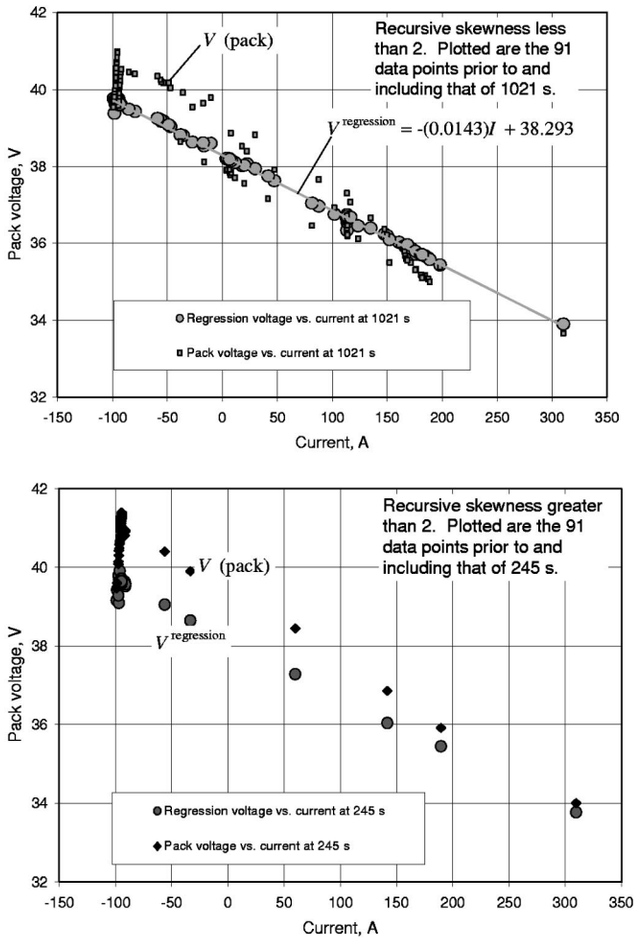

Figure 9. Recursive skewness analysis. The lower plot shows that at 245 s (see Fig. 7 for the measured current), the current is skewed, as a longer duration of dominantly constant charge currents are followed by a discharge. The clustering of currents at −100 A (charge) shown in the lower plot yields a skewed data set for linear regression. The maximum in the recursive skewness curve of Fig. 8 corresponds to the lower plot. In contrast, the more random current history associated with the upper plot yields good regression statistics.

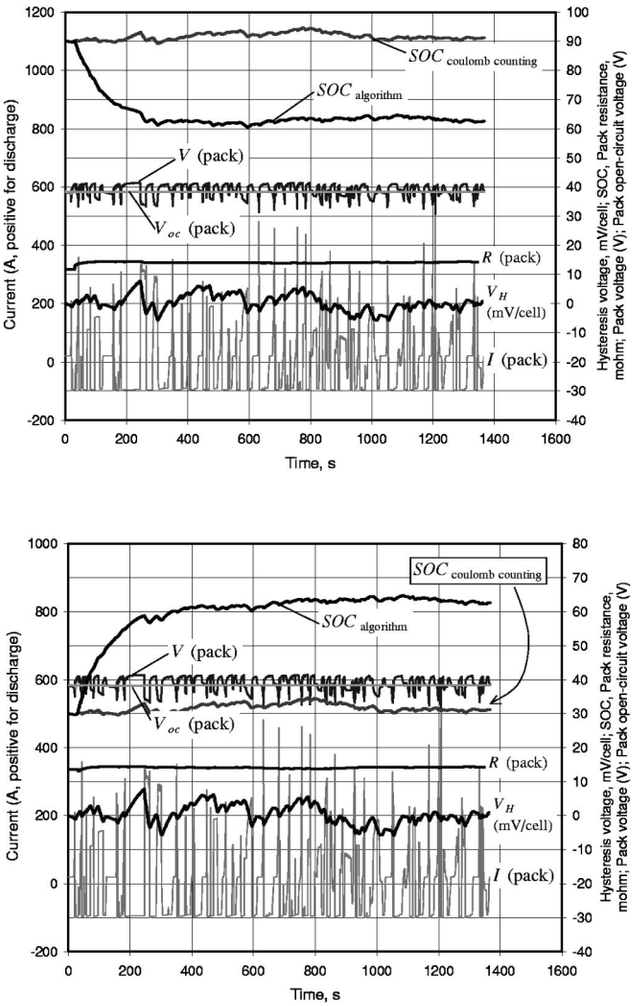

Figure 10. Algorithm convergence test. For the upper plot, the initial SOC was set to 90% (the correct value being 60% as in Fig. 7). For the lower plot, the initial SOC was set to 30%. A comparison with Fig. 7 shows that the algorithm converges to the correct SOC within about 200 s. Note that the regressed value for the high-frequency resistance value is not affected substantially.

ness in the current excitation source is less than 10 worked well.

The convergence of the algorithm is highly dependent on the value of the weight factor w_{SOC}. The voltage-based portion of the SOC calculation, SOC_V, converges rapidly, but it is highly sensitive to variations in the battery voltage; such variations can be attributable to both measurement and model errors, and these errors can give rise to unwanted instabilities in SOC_V. Conversely, the coulomb-counting-based portion of the SOC calculation, SOC_C, is a much more stable integral quantity, but it can steadily become inaccurate due to current efficiencies that are not known with enough certainty to be included in the model reference adaptive system. Thus, SOC_V contains the more adaptive portion of the algorithm, whereas SOC_C provides stability. For the base-case conditions chosen, the algorithm converges smoothly from intentionally erroneous starting values for the SOC in about 200 s, as indicated in Fig. 10. The initial value of *SOC* was 64% (cf. Fig. 7); the initial value for SOC was arbitrarily set to 90 and 30% for the upper and lower plots of Fig. 10, respectively. The results of Fig. 10 help to explain why a coulomb-counting SOC method cannot be used in actual vehicle applications. Any error in the SOC is not removed adaptively, and the pure coulomb-counting value for the SOC maintains at a value close to the erroneous initial starting value in each case. The power calculations are sensitive to the value of the SOC, as the driving force for discharge (respectively charge) power is the difference between the minimum (respectively maximum) voltage allowed and the V_{oc}, and V_{oc} is obtained from the value of *SOC*. Last, we note that the regressed high-frequency resistance *R* is not sensitive to erroneous values for *SOC* (compare Fig. 7 and 10), which bodes well for the use of an adapted high-frequency resistance as a diagnostic for a battery SOH.

A 25°C discharge power test of the algorithm for the PHT application is shown in Fig. 11. First, the power *vs.* time trace in the PHT over a drive similar to that of the Federal Test Procedure (FTP) was recorded. Then, in a separate laboratory test, six different max discharge power pulses were enforced at various times throughout the recorded FTP-like power cycle by setting the pack voltage to 30 V (10 V/module), indicated by the arrows in Fig. 11. Generally the predicted 2 s and instantaneous power calculations bounded the immediate discharge power available (cf. ovals), and the available power always exceeded the 2 s predicted power capability. These results are promising for vehicle integration, and similar results were obtained at −20 and 0°C.

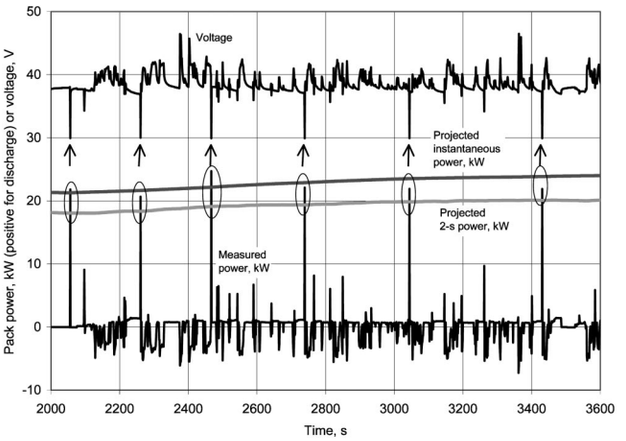

Figure 11. Discharge power test. Over an FTP-representative cycle recorded from a (GM) PHT drive, the pack voltage was set abruptly to 30 V (10 V/module) at six different times, as indicated by the arrows. Generally, the predicted 2 s and instantaneous power calculations bounded the immediate discharge power available (cf. ovals), and the available power always exceeded the 2 s predicted power capability.

As mentioned previously, the equivalent circuit shown in Fig. 4 should suffice to represent all known batteries for EV and HEV applications. The results shown in Fig. 12 and 13 support this assertion, as the data correspond to a high-voltage EV NiMH battery system. Because the SOC varies over a wide range in EV applications, in contrast to HEV applications, the high-frequency resistance R also shows variations, and the variation in R is generally consistent with published measurements of this quantity for NiMH EV battery modules.[13] Thus if R is to be used to determine a battery SOH in application, one must normalize the regressed value of R to nominal values which are a function of both temperature and SOC. For Fig. 12 and 13, the Ah capacity was determined before the discharges for the EV battery pack, so the coulomb-counting value for the SOC is accurate, and the difference between the regressed SOC and that obtained by coulomb counting corresponds to the algorithm error, which is sufficiently small for application purposes. In actual applications, the Ah capacity of the battery pack is not known prior to every drive, so an adaptive SOC algorithm is required. (The pack capacity can be estimated and updated adaptively for drives in which the pack is initially near full capacity and the final SOC and pack voltage are low.[12])

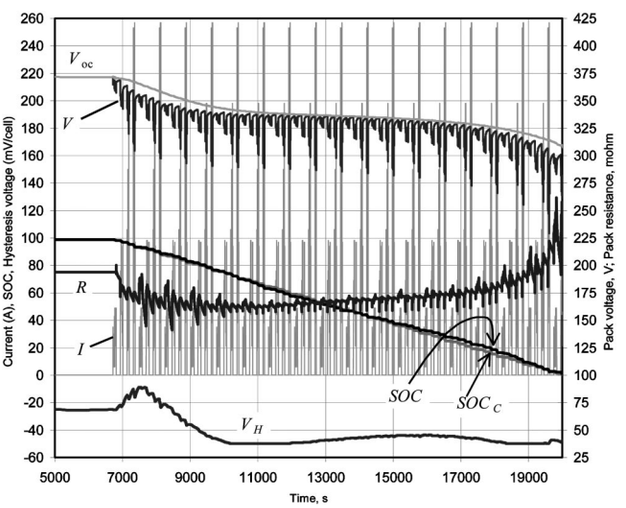

Figure 12. Weighted recursive least-squares algorithm applied to an electric vehicle (NiMH) battery pack of 26 modules. The pack was discharged through a resistor to yield the desired current excitation. For these data, $Ah_{\text{nominal}} = 105$, $\lambda = 0.95$, $\lambda = 1$, $\alpha_w = 0.001\ s^{-1}$, and $\alpha_H = 0.005\ s^{-1}$.

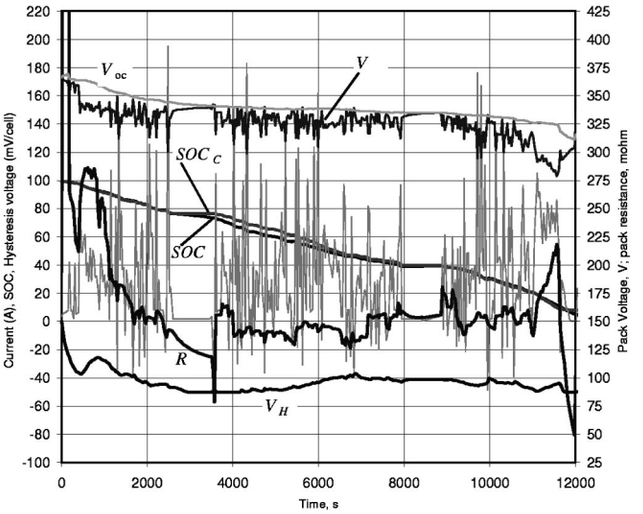

Figure 13. Algorithm applied to an S10E drive with the same battery pack as shown in Fig. 12. Parameters correspond to those of Fig. 12, with the exception that $\lambda = 0.9$; the value of λ was lowered to account for the larger time per point (30 s for this profile *vs.* 1 s in Fig. 12) and the corresponding need to reduce the impact of earlier (*i.e.*, relatively older than in Fig. 12) data points.

Conclusions

Efficient HEV and EV operation requires knowledge of the battery state; *i.e.*, how much energy is left in the battery and how much power the battery can discharge or accept. The algorithm derived and implemented in this paper represents a potential means to address these issues in an efficient manner consistent with the computational capabilities of embedded controllers employed by the automotive industry. The algorithm can be used on both lead-acid and NiMH traction battery systems and should work for other battery systems as well. It is suggested that the high-frequency resistance be used as a proxy for the SOH of the battery modules; determining the module SOH adaptively is important for optimal energy management and on-board diagnostics.

Acknowledgments

Many engineers and scientists at the GMNA Electrical Center and GM R&D contributed to this work. Robert Conell performed the power tests shown in Fig. 11. In addition, we had many insightful discussions with Ramona Ying, Bob Conell, and Robin Vidas.

General Motors Corporation assisted in meeting the publication costs of this article.

List of Symbols

Ah	coulombic capacity, C-h/s
A	$1/C_D$, F (Eq. 3)
b	Regressed intercept (Eq. 10)
B	$1/(R_{ct}C_D)$, 1/s (Eq. 3)
C_D	capacitance, F (cf. Fig. 4)
I	current, A
m	regressed slope (Eq. 10)
P	power, W
R	high-frequency resistance, ohms (cf. Fig. 4)
R_{ct}	effective interfacial resistance, ohm (cf. Fig. 4)
SOC	percent state of charge (energy content in the battery relative to the energy content upon full charge)
s	sum
t	time, s
V	system voltage, V

V_H hysteresis voltage, V (cf. Eq. 5 and Fig. 4)
V_{oc} open-circuit voltage, V (cf. Fig. 4)
w_H hysteresis weight factor (Eq. 19)
w_{SOC} weighting factor (Eq. 1)

Greek

β hysteresis parameter (Eq. 5)
ϵ self-discharge hysteresis parameter (Eq. 5)
η_I current efficiency (Eq. 2)

References

1. M. W. Verbrugge and E. D. Tate, *J. Power Sources*, **126**, 236 (2004); M. W. Verbrugge and E. D. Tate, in *Proceedings of the 3rd International Advanced Automotive Battery Conference*, Nice, France, June 10-13, 2003.
2. P. S. Maybeck, in *Mathematics in Science and Engineering*, Vol. 141-1, Academic Press, New York (1979).
3. *Applied Optimal Estimation*, A. Gelb, Editor, MIT Press, Cambridge, MA (1974).
4. B. Widrow and S. D. Stearn, *Adaptive Signal Processing*, Prentice-Hall, Englewood Cliffs, NJ (1985).
5. L. Ljnug and T. Söderström, *Theory and Practice of Recursive Identification*, MIT Press, Cambridge, MA (1986).
6. K. J. Aström and B. Wittenmark, *Adaptive Control*, Addison-Wesley, Reading, MA (1989).
7. R. Kulhavý, *Recursive Nonlinear Estimation. A Geometric Approach*, Springer, London (1996).
8. S. Pillar, M. Perrin, and A. Jossen, *J. Power Sources*, **96**, 113 (2001).
9. M. Verbrugge, E. Tate, S. Sarbacker, B. Koch, D. Frisch, and R. Ying, U.S. Pat. 6,639,385 (2003).
10. M. W. Verbrugge, S. Tarnowsky, R. Conell, and R. Ying, in *Proceedings Volume for the Advanced Automotive Battery Conference*, Las Vegas, NV, Feb 4-7, 2002.
11. See Power Assist Test Manual at http://www.uscar.org/consortia&teams/consortiahomepages/con-usabc.htm
12. M. Verbrugge, E. Tate, S. Sarbacker, and B. Koch, U.S. Pat. 6,359,419, (2002).
13. M. W. Verbrugge and R. S. Conell, *J. Electrochem. Soc.*, **149**, A45 (2002).
14. J. S. Dunning, Ph.D. Thesis, University of California, Los Angeles, CA (1971).
15. J. Newman and W. Tiedemann, *AIChE J.*, **21**, 25 (1975).
16. J. Newman, *Electrochemical Systems*, 2nd ed., Prentice-Hall, Englewood Cliffs, NJ (1991).
17. H. Bode, *Lead-Acid Batteries*, R. J. Brodd and Karl V. Kordesch, Translators, Wiley-Interscience, New York (1977).
18. M. W. Verbrugge, *AIChE J.*, **41**, 1550 (1995).
19. M. W. Verbrugge, D. W. Glander, and D. R. Baker, *J. Cryst. Growth*, **81**, 155 (1995).
20. C. Y. Wang, W. B. Gu, and B. Y. Liaw, *J. Electrochem. Soc.*, **145**, 3407 (1998).
21. D. R. Baker and M. W. Verbrugge, *J. Electrochem. Soc.*, **146**, 2413 (1999).
22. I. J. Ong and J. Newman, *J. Electrochem. Soc.*, **146**, 4360 (1999).
23. K. E. Thomas, R. M. Darling, and J. Newman, *Advances in Lithium-Ion Batteries*, Chap. 12, W. van Schalkwijk and B. Scrosati, Editors, Kluwer Academic/Plenum, Dordrecht (2002).
24. D. M. Bernardi and M. K. Carpenter, *J. Electrochem. Soc.*, **142**, 2631 (1995).
25. J. Newman and W. Tiedemann, *J. Electrochem. Soc.*, **144**, 3081 (1997).
26. M. W. Verbrugge, in *Proceedings from the 17th International Electric Vehicle Symposium*, Sec. 4B, Oct 2000.
27. *Standard Mathematical Tables*, 24th ed., W. H. Beyer, Editor, CRC Press, Cleveland, OH (1976).
28. P. Leblanc, C. Jordy, B. Knosp, and P. Blanchard, *J. Electrochem. Soc.*, **145**, 860 (1998).
29. P. Bernard, *J. Electrochem. Soc.*, **145**, 456 (1998).